

1995107823

324030

**FREE-TO-ROLL TESTS OF X-31 AND F-18 SUBSCALE
MODELS WITH CORRELATION TO FLIGHT TEST
RESULTS**

58-02

16086

P-28

David L. Williams II

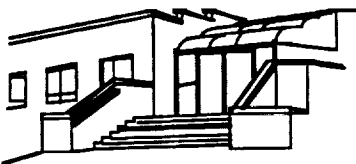
Robert C. Nelson

**Hessert Center for Aerospace Research
University of Notre Dame, Notre Dame, Indiana**

David F. Fisher

NASA-Ames Research Center

Dryden Flight Research Facility, Edwards, California



**The Hessert Center for Aerospace Research
Notre Dame, Indiana**

OUTLINE OF PRESENTATION

This presentation will concentrate on a series of low-speed wind tunnel tests conducted on a 2.5% subscale F-18 model and a 2% subscale X-31 model. The model's control surfaces were unaugmented; and for the most part, were deflected at a constant angle throughout the tests. The tests consisted mostly of free-to-roll experiments conducted with the use of an air-bearing, surface pressure measurements, off-surface flow visualization, and force-balance tests. Where possible the results of the subscale tests have been compared to flight test data, or to other wind tunnel data taken at higher Reynolds numbers.



THE HESSERT CENTER

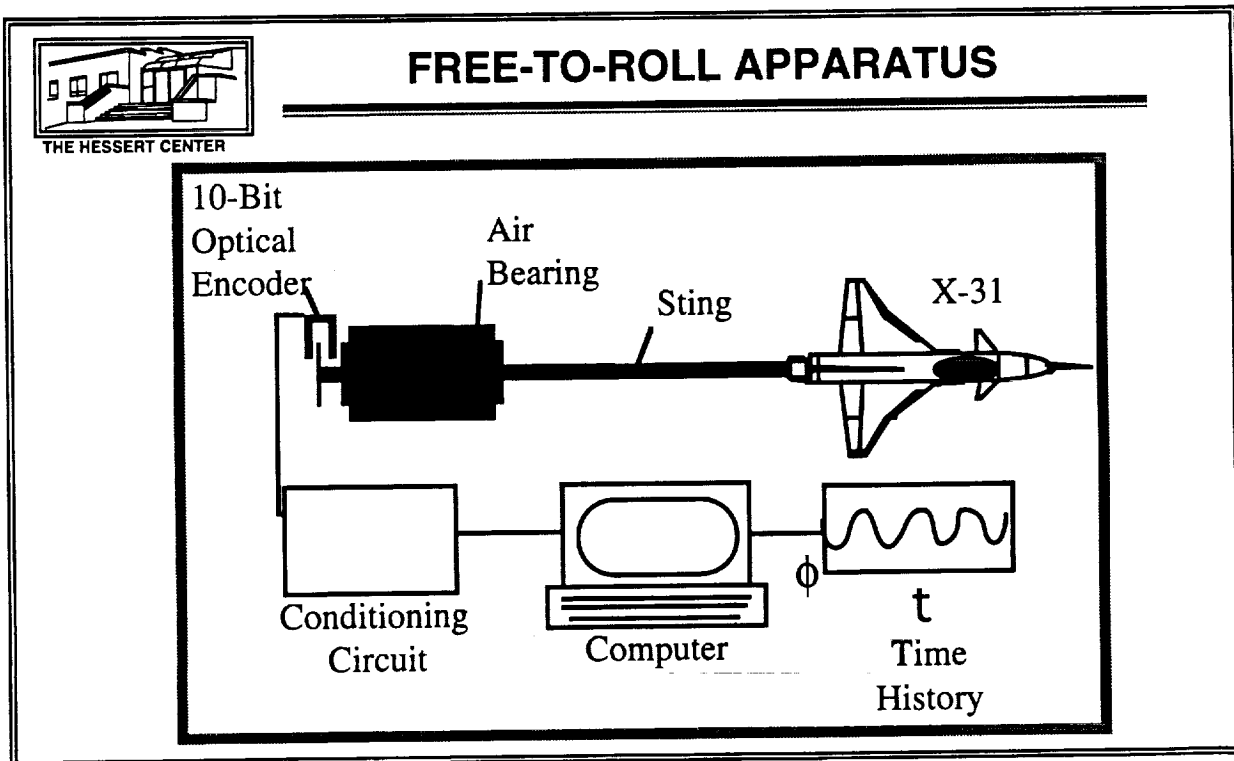
OUTLINE OF PRESENTATION

- **Experimental Procedures and Equipment**
- **F-18 and X-31 Model Configurations**
- **Self-Induced Motion Envelopes of Models Versus Flight Tests or Drop Model Tests**
- **Vortex Behavior During Self-Induced Motions**
- **Reynolds Number Issues for Dynamic Roll Experiments**
- **Concluding Remarks**

FREE-TO-ROLL APPARATUS

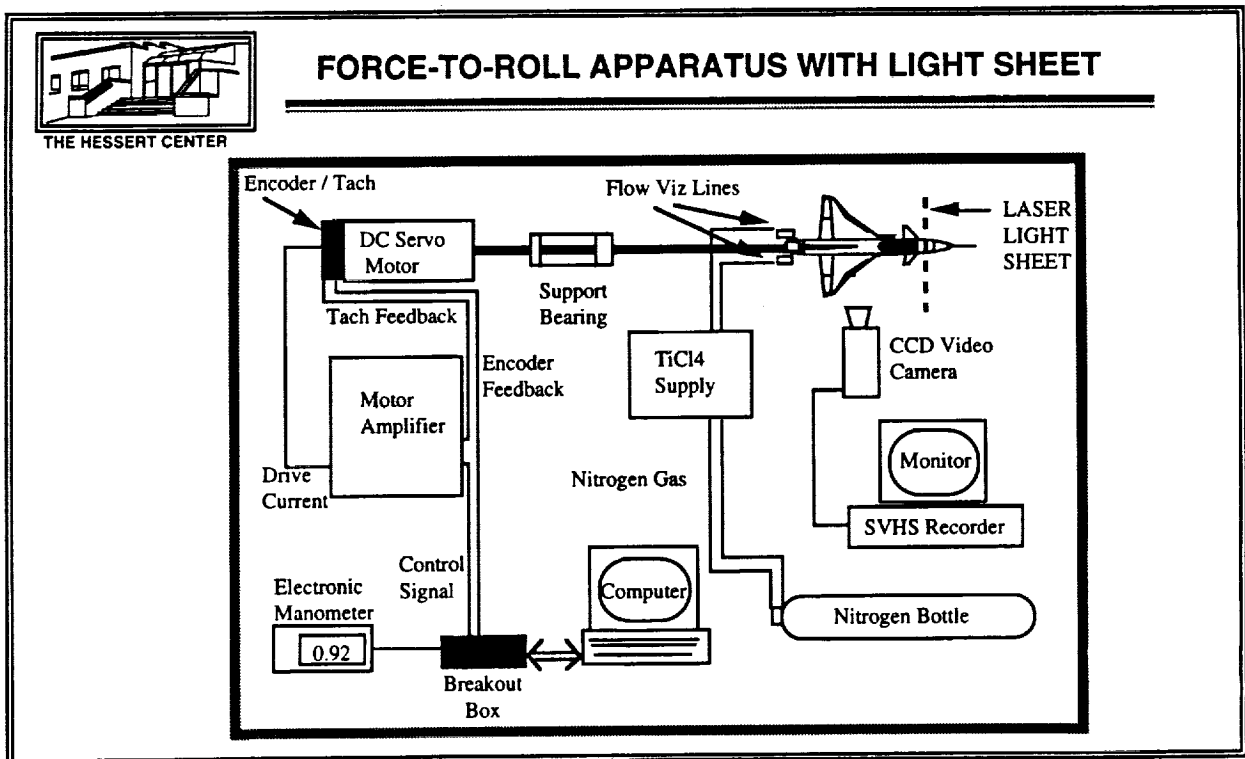
Two unique experimental apparatus have been developed at the University of Notre Dame to study the wing rock characteristics of slender wings and subscale models. The systems consist of a free-to-roll apparatus which is used to measure the rolling histories of a model in the absence of bearing friction, and a controlled motion apparatus for flow visualization and unsteady surface pressure measurements.

A schematic of the free-to-roll apparatus may be seen below. This apparatus was designed to allow for a simulation of the free flight environment for a single-degree-of-freedom. At the heart of the apparatus is the air bearing spindle. The air bearing reduces the bearing friction within the system by an order of magnitude over that achieved with low friction ball bearings. Thus, the free-to-roll system allows the isolation of aerodynamic roll moments acting on the model. Instantaneous roll angle is provided by a 10-bit modular, optical encoder yielding an angular resolution of 0.35° . The use of the modular encoder eliminates any friction in the roll measurement process. The time histories from the encoder are stored and may be used to estimate angular velocity, acceleration, and aerodynamic rolling moments.



FORCE-TO-ROLL APPARATUS WITH LIGHT SHEET

To obtain dynamic flow visualization data on a model undergoing wing rock, a unique motion control / data acquisition system is used. The motion control system is necessary due to smoke injection tubing for flow visualization, and the wire leads from the pressure transducers to the data acquisition computer. The tubes and transducer leads eliminate the free-to-roll nature of the system. A sketch of the system may be seen below. Motion control is accomplished with a DC servo motor connected to a motor amplifier and motion control computer board. Tachometer and encoder signals are used for feedback. The motion controller uses high-speed digital processing and has an accuracy of ± 1 count in 10,000 (0.036°). Digital proportional-integral-derivative (PID) with velocity and acceleration feedforward control is implemented for precision tracking of the time history. All gains are user adjustable so that the system may be fine-tuned for a given model. The servo motor is connected to the model via a sting which rides on conventional ball bearings. Time histories taken with the free-to-roll apparatus were used to provide the input signal to the motion control system to drive the model through the self-induced roll oscillation trajectories. The system accurately reproduces a free-to-roll time history while allowing for an instrumented model to be used.

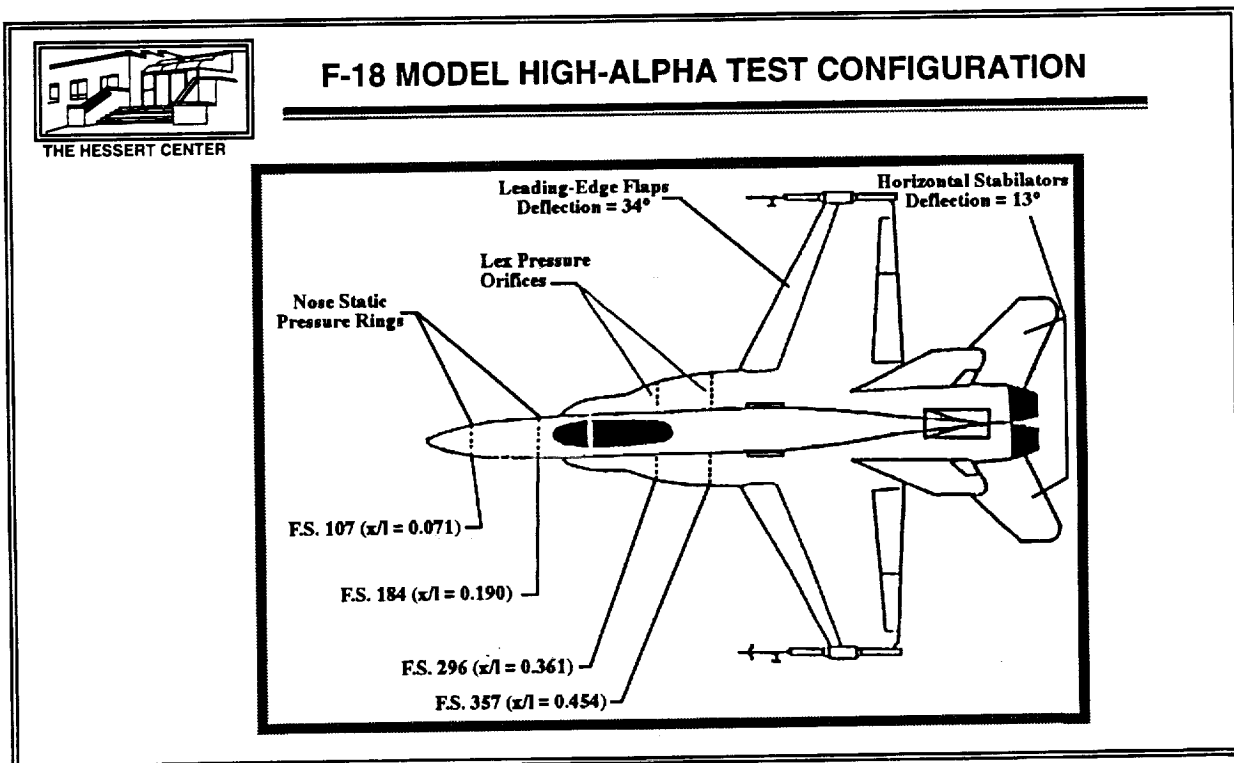


F-18 MODEL HIGH-ALPHA TEST CONFIGURATION

The F-18 model used in these experiments was a 2.5% (1/40th) scale model. Since the model contained stationary flight control surfaces, these were deployed to represent a correct configuration of the HARV vehicle in high-alpha flight conditions. The leading-edge flaps were set to a fixed 34° down since all investigations were at angles-of-attack greater than 20°. In addition, the horizontal stabilators were fixed at a positive 13° rotation which represents a mean deflection over the angle-of-attack range tested. All other control surfaces were set to 0° deflection.

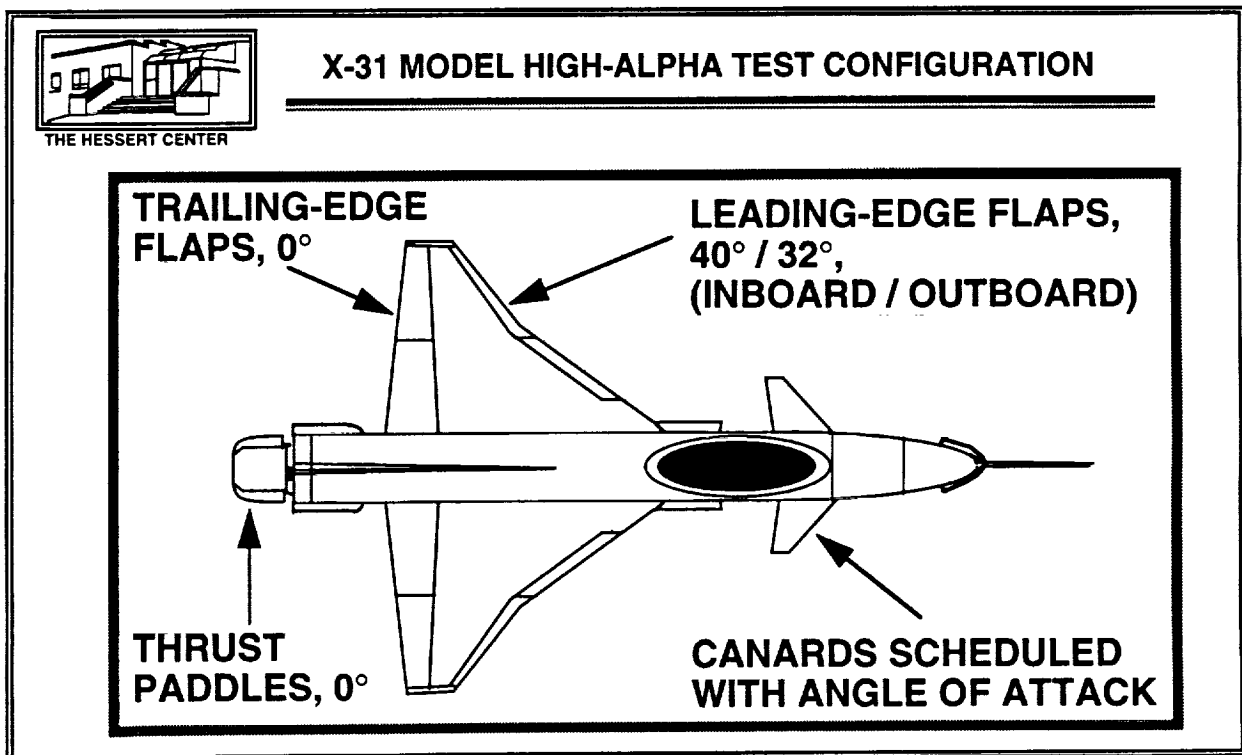
In order to investigate the surface pressures existing on the subscale model during testing, static surface pressure taps were installed at several fuselage stations (F.S.) corresponding to those tested on the HARV vehicle. Due to the small size of the model, the number and spacing of these static pressure taps at each fuselage station was constrained; however, enough were installed to allow comparison of the surface pressures on the 2.5% model to similar measurements completed on the HARV vehicle⁶.

Lastly, to investigate off-surface flow structures, internal flow visualization ports were installed in the forebody and LEX's of the model.



X-31 MODEL HIGH-ALPHA TEST CONFIGURATION

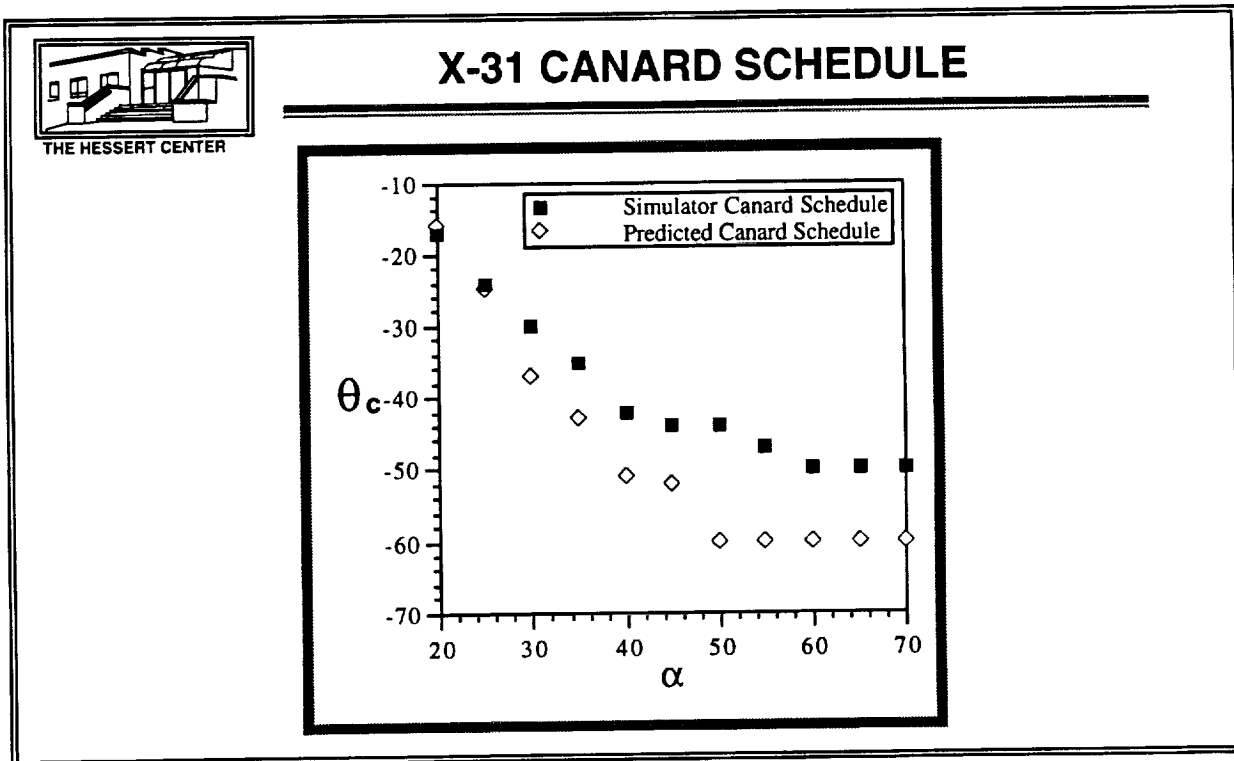
The X-31 model used in the experiments was a 2% scale modified desktop model. It contains both the nose-strakes and empennage strakes found on the X-31 aircraft. The nose strakes installed on the model were 0.394 inches (19.7 inches full-scale). Control surface deflection data for the X-31 during level flight at high angle-of-attack and for an $\alpha = 0^\circ$ to 70° pitch-up maneuver from the X-31 simulator were used to obtain each control surface deflection angle. The leading-edge flap was permanently deflected to $\theta_{LE} = 40^\circ/32^\circ$, (inboard/outboard) flap deflection, since this is the flap schedule for the X-31 aircraft for any $\alpha \geq 27^\circ$. The trailing-edge flap and thrust paddles were set to 0° deflection for all tests. Lastly, the canards on the model were made fully positionable and scheduled with respect to angle of attack as noted above.



X-31 CANARD SCHEDULE

The X-31 canard surfaces were scheduled with respect to angle of attack for each of the tests conducted on the model. Once the model was secured on its sting at a given angle of attack, the canard was fixed at its scheduling value according to the graph below.

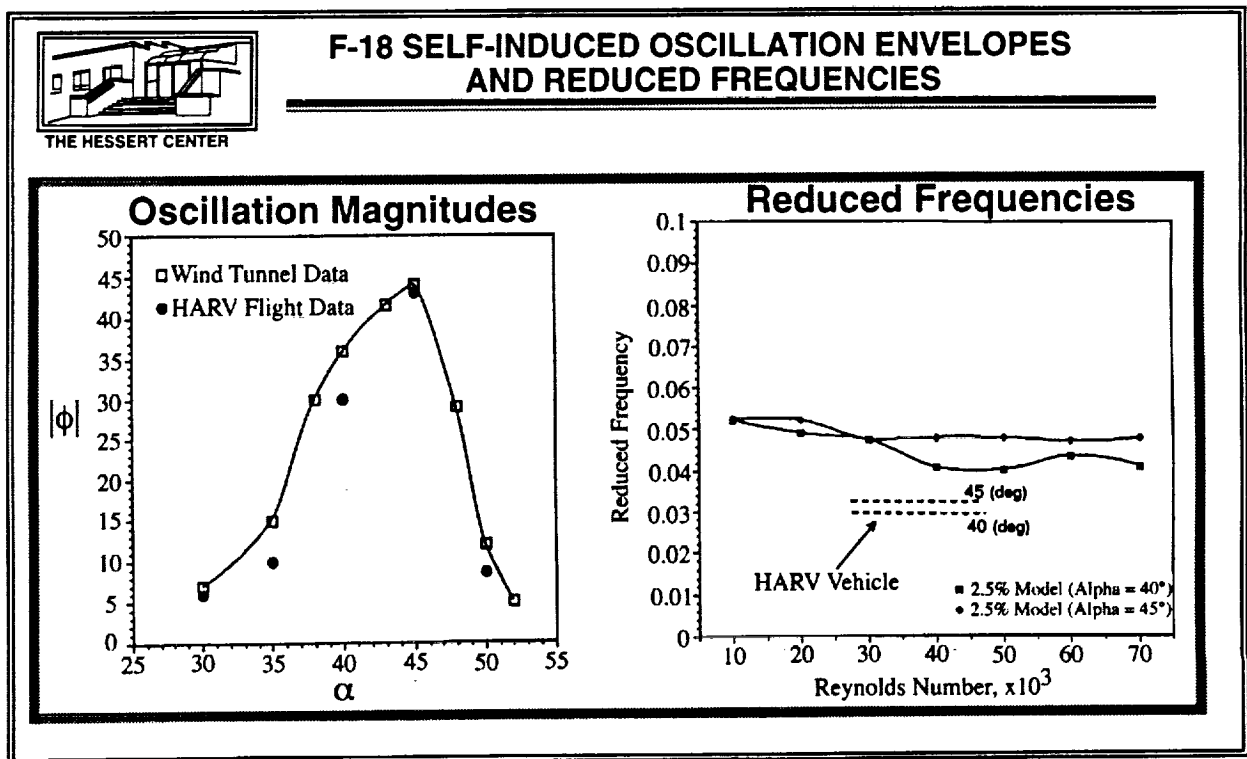
As can be noted, there are two schedules. The first is the canard schedule for an $\alpha = 0^\circ$ to 70° pitch-up maneuver from the X-31 simulator; and, the second is a predicted canard schedule for level flight¹³. For both schedules, a negative value indicates a leading-edge down and trailing-edge up rotation of the canard. Prior to testing it was expected that both schedules would produce similar results in the free-to-roll tests; however, this was not the case. Thus, all tests were repeated for both schedules.



F-18 SELF-INDUCED OSCILLATION ENVELOPES AND REDUCED FREQUENCIES^{11, 12}

The 2.5% F-18 model was tested with the free-to-roll apparatus over $\alpha = 25^\circ$ to 70° with $\beta = 0^\circ$. The model was released from a stationary position of $\phi = 0^\circ$ at each angle of attack and the ensuing model motion recorded.

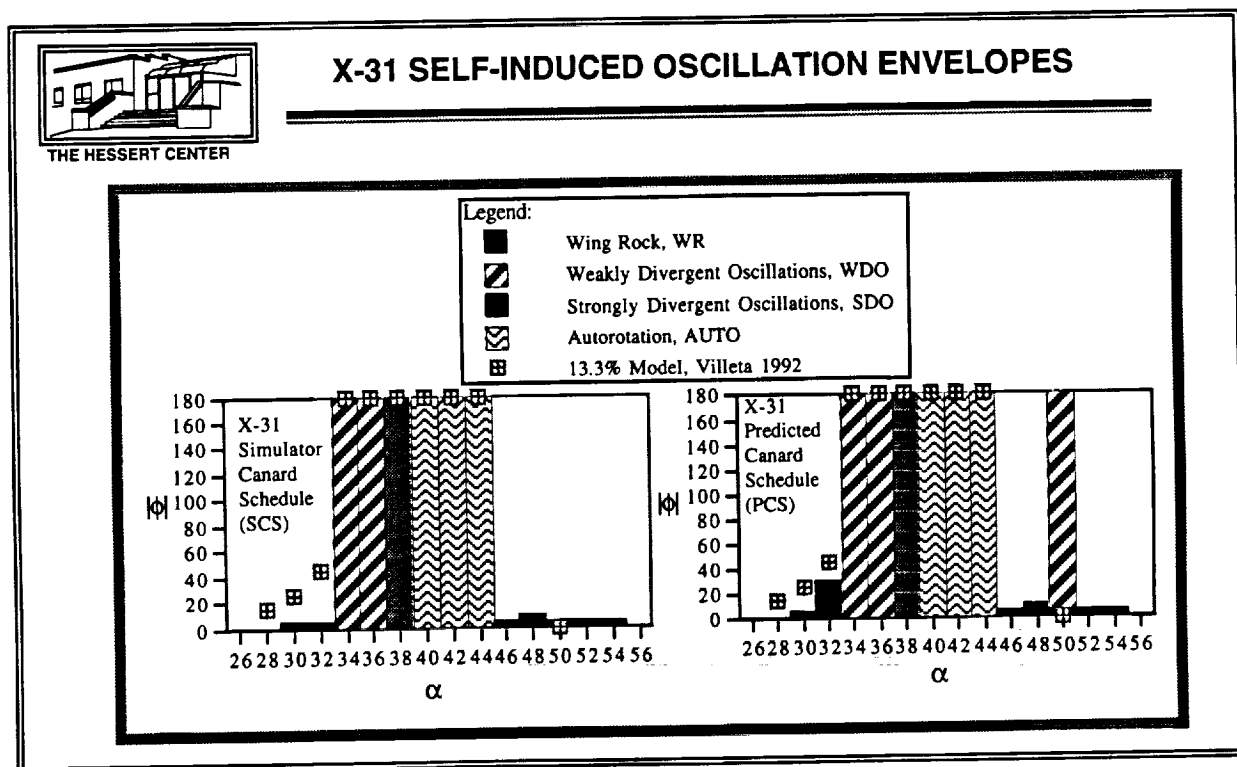
The comparison of wind tunnel and flight test data for the amplitude envelope and reduced frequencies are shown below^{11, 12}. The data shows good agreement in several areas. The first area of agreement is the general trend of the wing rock envelope. Both flight test and wind tunnel data show a rising trend in the wing rock amplitude between $\alpha = 30^\circ$ and 40° . The peak motion occurs at $\alpha = 45^\circ$, after which there is a sharp drop-off in the wing rock motion. Along with the comparable envelope shape, the amplitudes of the data compare reasonably well within the uncertainty of estimating the HARV wing rock amplitudes. This plot helps to identify one area of subscale utility, that being the ability to identify regions in which a particular phenomenon will occur. In this case, it is obvious that there is a range of angle of attack (40° - 47°) where robust wing rock motion occurs. Additionally, it is possible to predict the magnitude of this motion as can be seen from the close correlation in the data. The reduced frequencies of the wing rock motions are also similar; although, the 2.5% model values are slightly higher in value than the HARV vehicle.



X-31 SELF-INDUCED OSCILLATION ENVELOPES

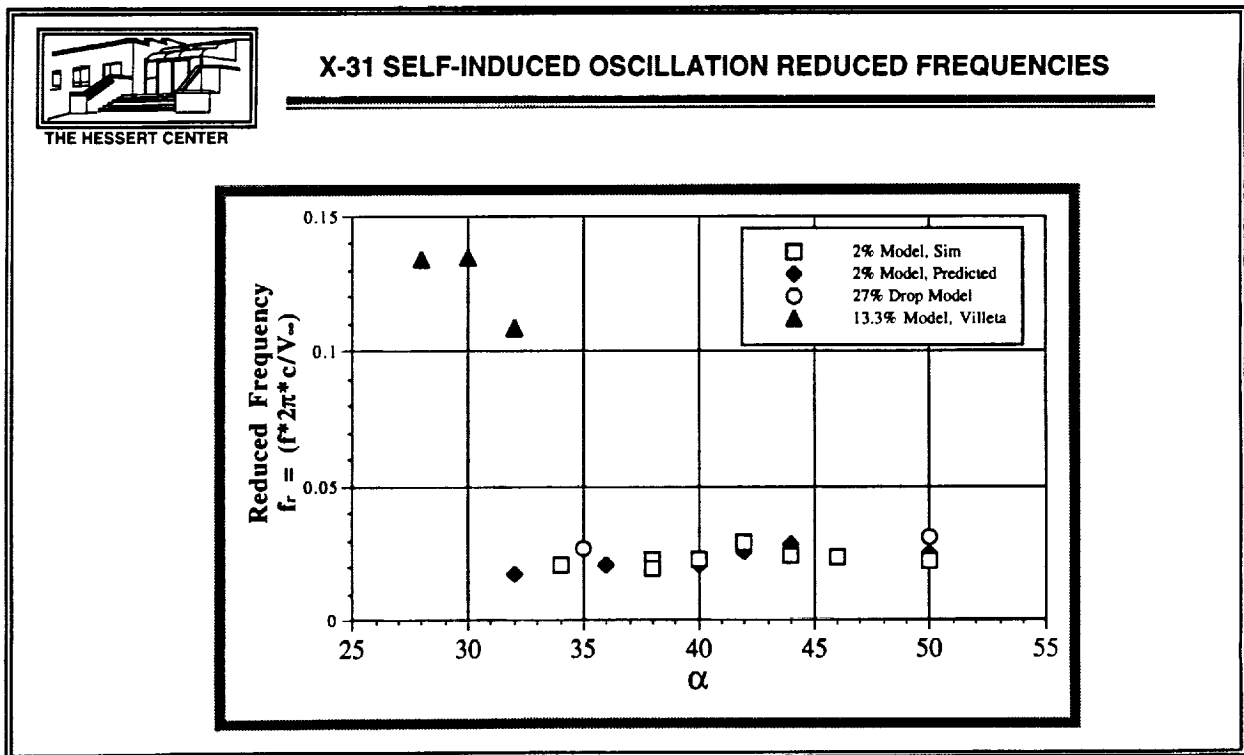
The 2% subscale X-31 model was tested with the free-to-roll apparatus, discussed in the previous section, over $\alpha = 25^\circ$ to 70° with $\beta = 0^\circ$. For each individual case, the model was released from a stationary position of $\phi = 0^\circ$ at each alpha and the resulting model motion recorded. The results of these tests showed several aerodynamic phenomenon occurring with the model. As can be noted from the graphs below, several phenomena occur in the alpha range of 30° to 55° for both canard schedules¹³. In addition, the magnitudes compare favorably to tests conducted by Villeta in 1992 on a 13.3% X-31 model¹⁴. The model did experience wing rock (WR) during the tests; however, most of the envelope was found to be divergent motions. In the divergent portion of the oscillation envelope, $\alpha = 34^\circ - 44^\circ$, three types of divergent motion occur. These are weakly divergent oscillations (WDO), strongly divergent oscillations (SDO), and autorotation (AUTO). In addition, Villeta showed in 1992 that the wing rock and autorotation phenomena experienced by the 27% X-31 drop model were essentially one degree-of-freedom motions¹⁴.

Comparison to the X-31 flight vehicle is not possible due to the highly integrated flight control system on the aircraft. Thus, comparisons are made with X-31 free-flight model tests and other wind tunnel tests.



X-31 SELF-INDUCED OSCILLATION REDUCED FREQUENCIES

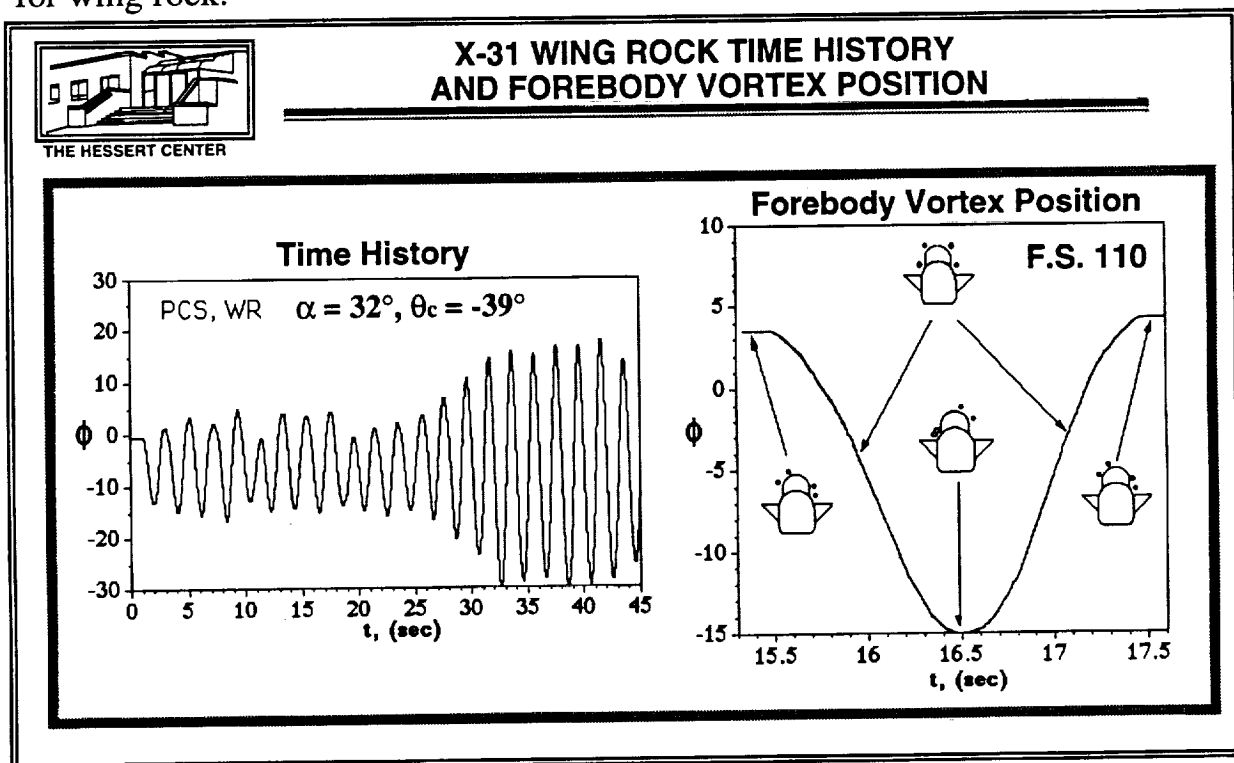
The recorded free-to-roll time histories of the 2% X-31 model also revealed the reduced frequencies of the oscillations motions. These values are shown below with corresponding information from two other X-31 subscale model tests. The values from the 2% X-31 model match well with the 27% X-31 drop model tests conducted at the Plumtree Test Facility of Langley Research Center, reported by Villeta¹⁴. In this case, the 2% X-31 model values are only slightly lower than the 27% X-31 drop model. However, there are some discrepancies between the values when compared with those found by Villeta during low-speed wind-tunnel tests of a 13.3% X-31 model. The values shown for the 13.3% model are the only ones given in Villeta's paper¹⁴. Since the X-31 flight vehicle has such a highly integrated flight control system, it does not experience the oscillations necessary for comparison. Thus, the drop model tests may provide the only source of information near the X-31 aircraft's flight conditions.



X-31 WING ROCK TIME HISTORY AND FOREBODY VORTEX POSITION

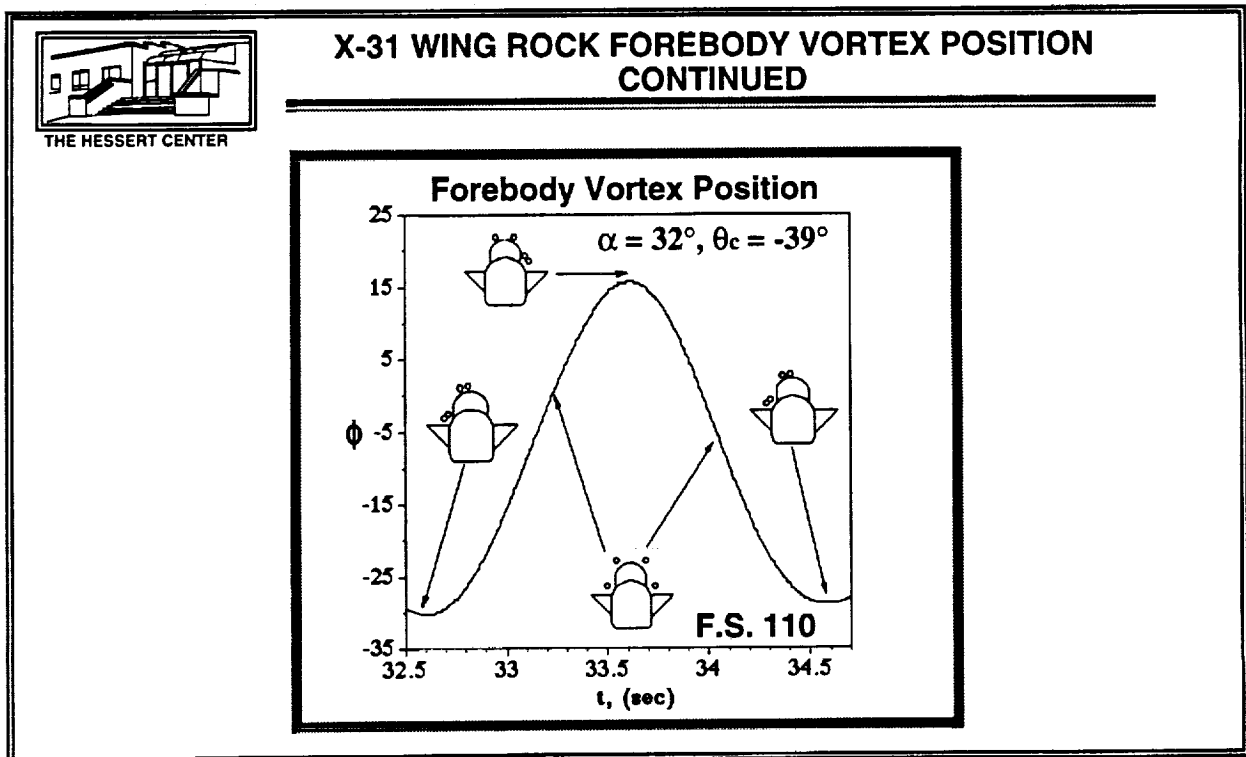
As the angle of attack is increased, the first phenomenon encountered is wing rock, WR¹³. This is a self-induced, limit-cycle roll oscillation seen previously on many other aircraft and studied extensively during the past few years with the HARV program. As with other aircraft models, the wing rock encountered on the X-31 is not very smooth during its limit-cycle build-up or its maximum roll angle oscillations, see below. In addition, it should be noted that the values of peak-to-peak wing rock amplitude, $|\phi|$, are different for the two canard schedules. At this angle of attack, the wing rock amplitude values differ by 25°; however, the only difference between the two tests was a 7° difference in canard setting. Thus canard position is a factor in the aircraft's behavior, and this point was found numerous times throughout testing. Another unusual behavior found in X-31 wing rock is observed below. For some cases of wing rock, the model does not oscillate about a $\phi = 0^\circ$ roll angle. As shown below, an offset bias of the wing rock motion is observed in these cases. Both positive and negative offsets were recorded.

The forebody vortices and canard-fuselage junction vortices are shown for a portion of the wing rock cycle. At this stage in the build-up, the vortices pair at the highest roll angles and remain on their respective sides of the canopy. It is possible that interaction between the vortices may provide the instability needed for wing rock.



X-31 WING ROCK FOREBODY VORTEX POSITION CONTINUED

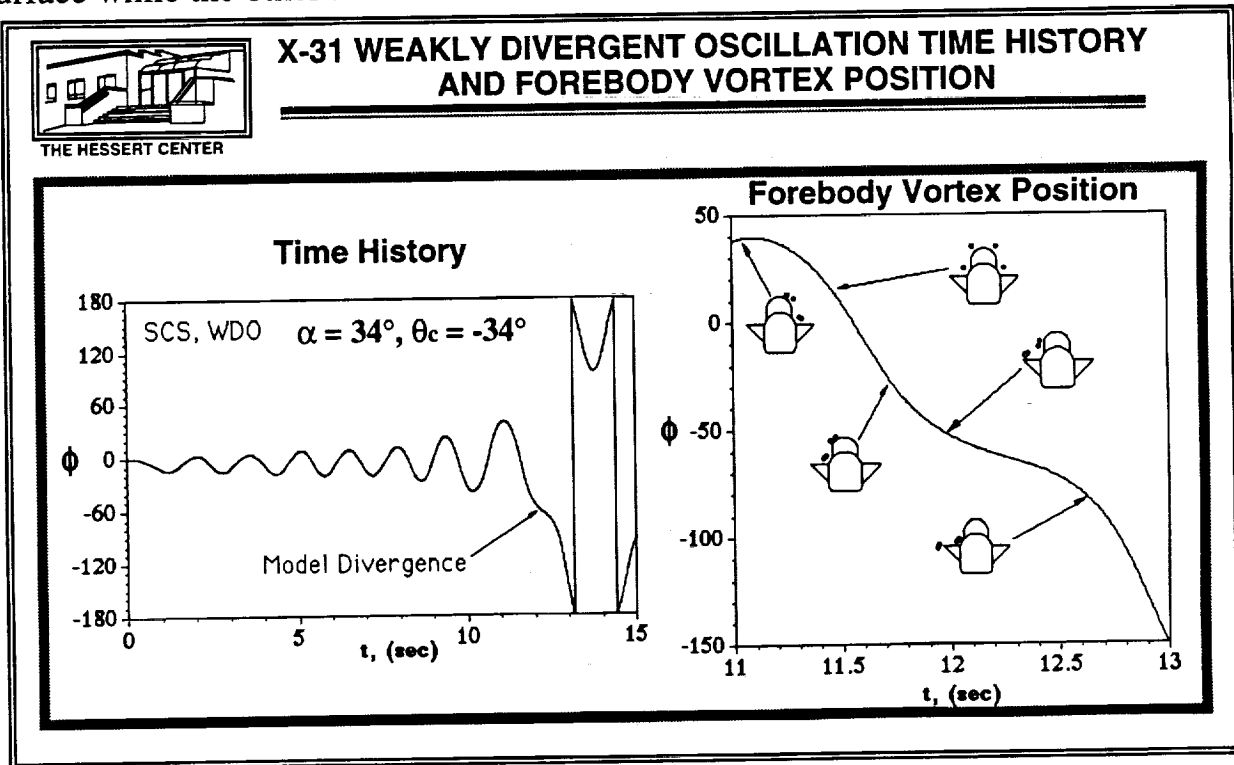
The figure below shows the position of the primary forebody vortices and canard-fuselage junction vortices during a large amplitude wing rock episode taken from the previous wing rock time history¹³. The motion of the forebody and canard-fuselage junction vortices is very similar to that seen for the small amplitude wing rock case discussed previously, with one exception. For the large amplitude wing rock case, the opposite side vortices move over the canopy to interact with the other vortex pair. This can be seen in the position of the vortices in this figure versus the position of the vortices shown previously for small amplitude wing rock. This movement of vortices across the top surface of the model is what separates large amplitude wing rock oscillations, $|\phi| > 30^\circ$, and small amplitude wing rock motions, $|\phi| \leq 15^\circ$. Again, the forebody vortices and the canard-fuselage junction vortices interact with each other during the wing rock motion.



X-31 WEAKLY DIVERGENT OSCILLATION TIME HISTORY AND FOREBODY VORTEX POSITION

Between $\alpha = 34^\circ - 36^\circ$, a motion occurs that has been termed a weakly divergent oscillation, WDO¹³. This motion is characterized by a long, slow oscillation build-up period which eventually leads to a roll divergence of the model, see below. In examining the time history, the long gradual build-up can be observed from 0 to approximately 11.5 seconds. Near 11.5 seconds, the model diverges near $\phi = -60^\circ$, and the aircraft continues its rolling motion into an inverted hung stall.

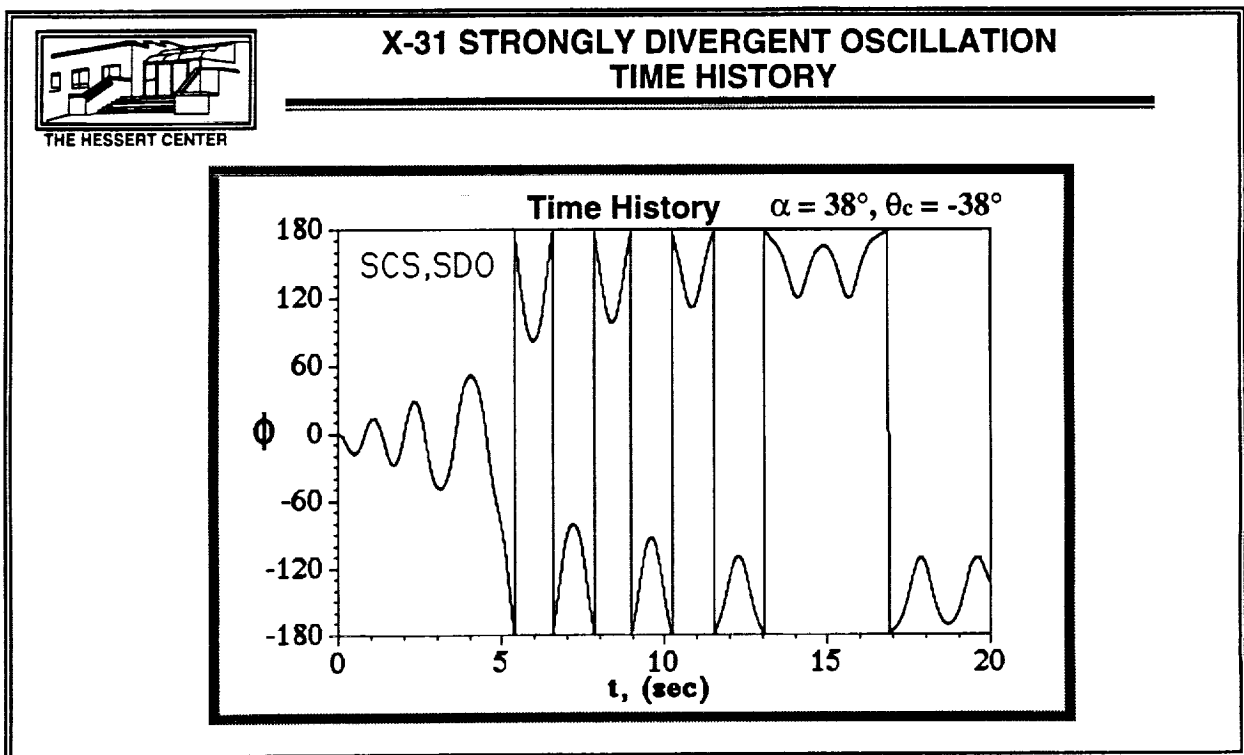
The forebody vortex position graph shows the position of the primary forebody vortices and canard-fuselage junction vortices during a weakly divergent oscillation episode, WDO, from the time history. The vortex motion prior to the divergence is similar to the wing rock discussed previously. Once the model starts to diverge, however, there is a marked difference. The vortex position at ~ 11 seconds is similar to that of large wing rock motions. As the model rolls through its neutral position (0°), ~ 11.4 seconds, the vortices separate and move around the canopy. As the model rolls further, ~ 11.7 seconds, the vortices again pair and move over the top of the canopy. Instead of returning back to its neutral position, however, the model continues to roll and diverge. At ~ 12 seconds, one vortex pair has moved out behind the surface of the canard while the second pair has begun moving down toward the same canard surface. Thus both pair are now acting solely on the same side of the model. As the model rolls further, ~ 12.6 seconds, one pair of vortices has moved behind the tip of the canard surface while the other has moved behind the canard root.



X-31 STRONGLY DIVERGENT OSCILLATION TIME HISTORY

As α continues to increase, a motion termed a strongly divergent oscillation (SDO), occurs near $\alpha = 38^\circ$. As opposed to the weakly divergent oscillation, this motion is characterized by a quick and violent oscillation build-up which rapidly leads to a roll divergence of the aircraft into an inverted hung stall. From the figure below, this quick roll divergence motion can be observed as the model's oscillations quickly build between 0 and 4.5 seconds and diverges afterward into an inverted flight condition. The SDO build-up to divergence occurs in most cases more than twice as fast than similar WDO cases. In addition, this model condition is not merely a low Reynolds number phenomena since the stabilization of the X-31 configuration into an inverted hung stall has been reported from previous high Reynolds number, subscale drop model tests¹⁴.

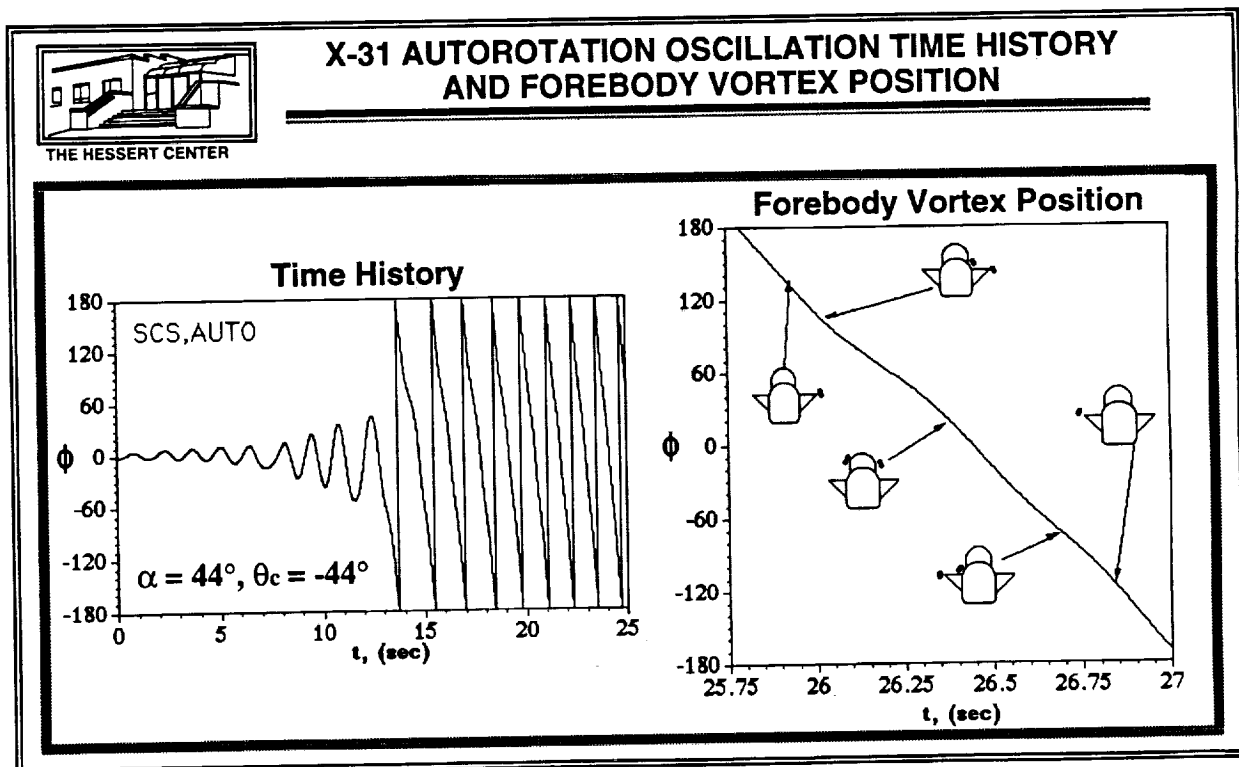
The movement of the forebody vortices and the canard-fuselage junction vortices are similar for both a SDO build-up and a WDO build-up. The only difference seems to be the time needed to build to divergence.



X-31 AUTOROTATION OSCILLATION AND FOREBODY VORTEX POSITION

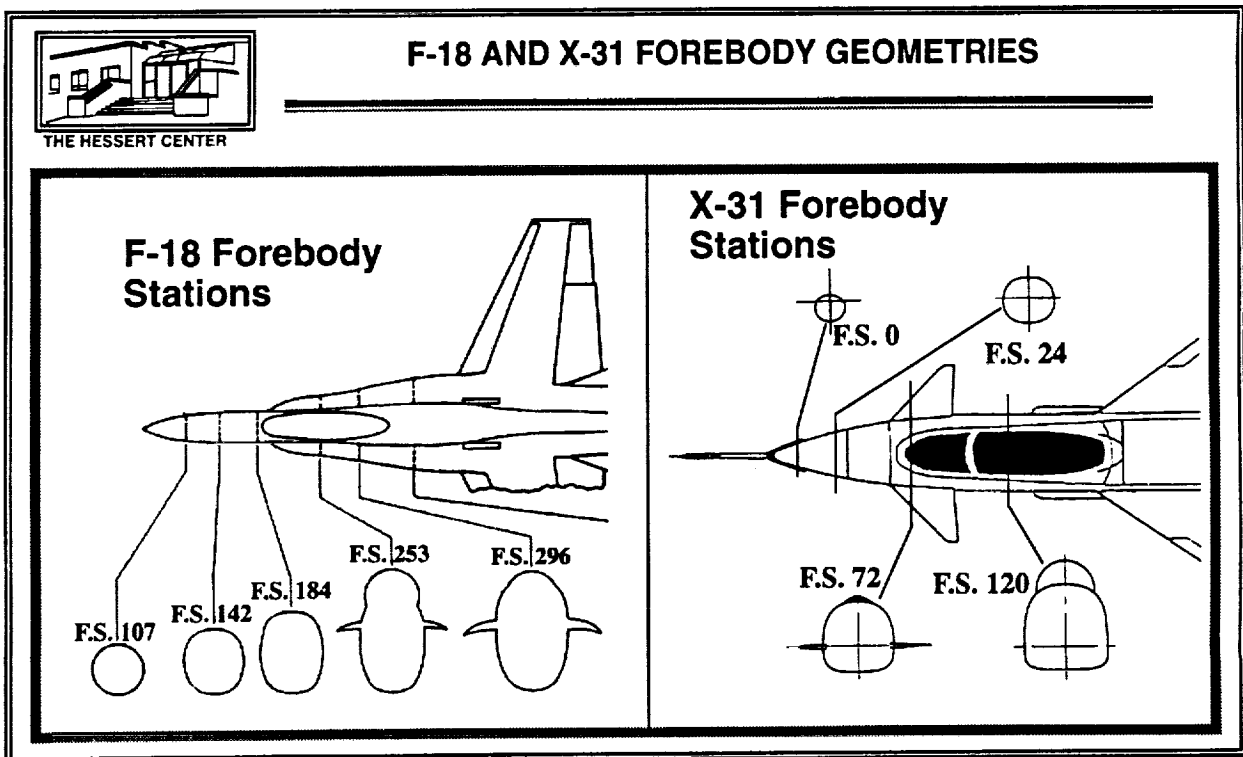
The last type of divergent motion encountered, as alpha continues to increase, is an autorotation divergence motion¹³, also term a High Incidence Kinetic Roll departure or HIKR departure. This motion is found at $\alpha = 40^\circ - 44^\circ$ for both canard schedules. It is characterized by a roll oscillation build-up that diverges into an autorotating motion. Once in the autorotating mode, the vehicle continues to spin, in one roll direction only, while the angular velocity increases to some limiting value, 0.85 Hz for the time history below. This type of behavior has also been reported during the X-31 drop model tests^{1, 14}.

The forebody vortex position graph shows the position of the primary forebody vortices and canard-fuselage junction vortices during the autorotation episode. At this point, the model has already diverged and is continuously rolling in one direction. One difference to be noted is that the vortices move quickly and efficiently across the upper surface of the model during this motion. In addition, they seem to move around the surface of the canards as well.



F-18 AND X-31 FOREBODY GEOMETRIES

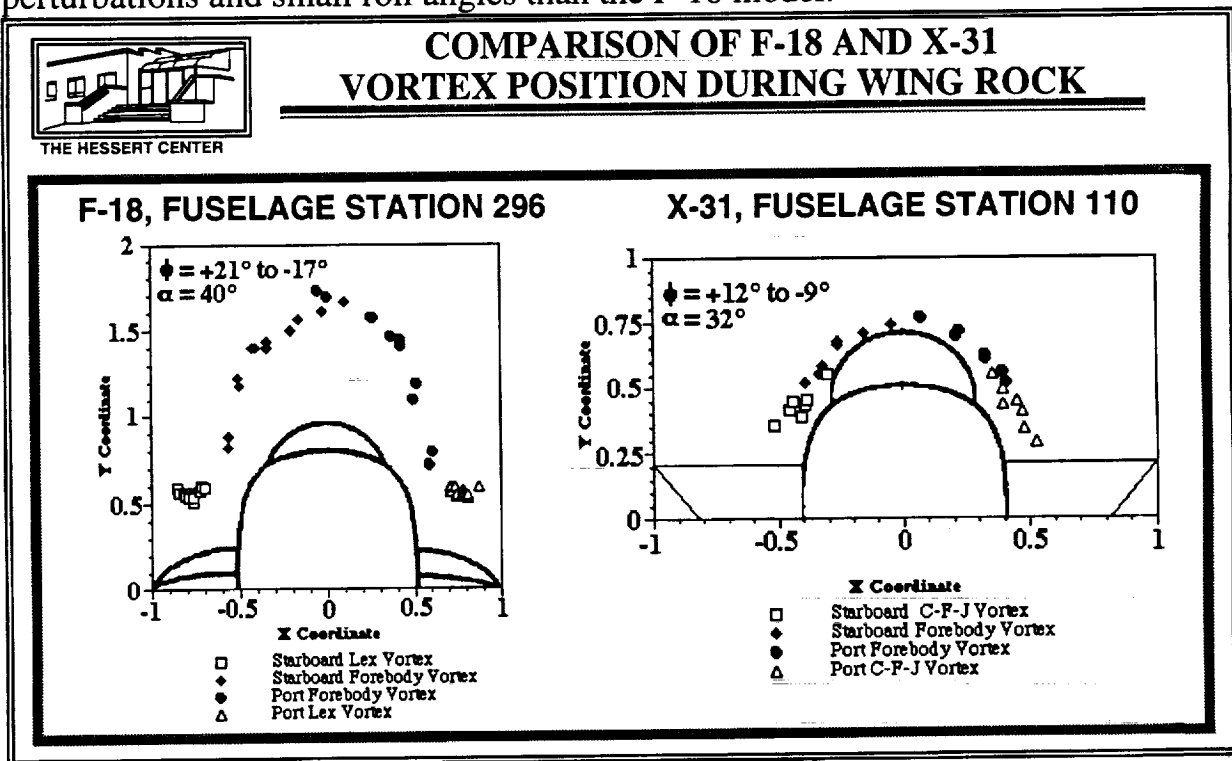
The forebody geometries of the F-18 and X-31 models are different from each other. The l/d ratio of the F-18 forebody is larger than that for the X-31. In addition, the X-31 model has a nose boom which is not present on the F-18. The cross-sections of the forebodies are different also. Both the F-18 and the X-31 start out with circular cross-sections, F.S. 107 (F-18) and F.S. 0 (X-31); however, the forebodies change at the latter fuselage stations. Comparing F.S. 184 of the F-18 and F.S. 24 of the X-31, we can note a difference in shape that will affect vortex strength and stability. Kegelman and Roos showed in 1991 that forebody cross-sections such as F.S. 24 of the X-31 will produce stronger forebody vortices than the cross-section of F.S. 184 of the F-18⁷. In addition, the vortices generated from cross-sections like F.S. 24 will experience greater lateral and normal movement due to flowfield perturbations than vortices generated by cross-sections like F.S. 184. Lastly, the two models have different placements of their canopies. The canopy on the F-18 has a high profile as seen in the cross-section of F.S. 253. The canopy on the X-31 has low profile as seen in the cross-section of F.S. 120. Aerodynamically, these canopies can act as physical barriers to separate the forebody aerodynamics and prevent interaction.



COMPARISON OF F-18 AND X-31 VORTEX POSITION DURING WING ROCK

When the activity of the foreword vortices during wing rock are compared for both the F-18 and X-31 subscale models several differences are observed. The two graphs shown below were picked for their similarity in forebody vortex lateral position (X-coordinate) during wing rock. In addition, the model conditions for each of these graphs has a maximum oscillation peak-to-peak amplitude of approximately 32° . However, there are three important differences between these graphs.

First, the magnitude of the roll angles needed to produce similar lateral movement should be observed. It takes nearly twice the roll angle of the X-31 model to produce the same magnitude of forebody vortex lateral movement on the F-18 model. Thus, forebody vortex movement is more prominent on the X-31 model. Second, the distance between the model surface and the forebody vortices (Y-coordinate) during wing rock are different. Since those of the X-31 model stay very close to the surface, it can be observed that they can have more of an affect on the model's behavior than its counterparts on the F-18 model. Lastly, the LEX vortices of the F-18 model are relatively stable during wing rock when compared to the canard-fuselage junction vortices of the X-31. Thus vortex interactions on the X-31 model are more prevalent and are not confined to a localized area. From this evidence it seems that the X-31 forebody configuration is more susceptible to perturbations and small roll angles than the F-18 model.



COMPARISON OF F-18 AND X-31 VORTEX POSITION DURING PITCH MANEUVERS

Both models were tested using pitch maneuvers to locate any instabilities that might initiate self-induced oscillations. These pitch maneuvers included ramp motions from $\alpha = 10^\circ - 60^\circ$ and sinusoidal pitch motions using various angle-of-attack ranges with varying frequencies of oscillation. Tests were conducted with $\beta = 0^\circ$ and $\phi = 0^\circ$.

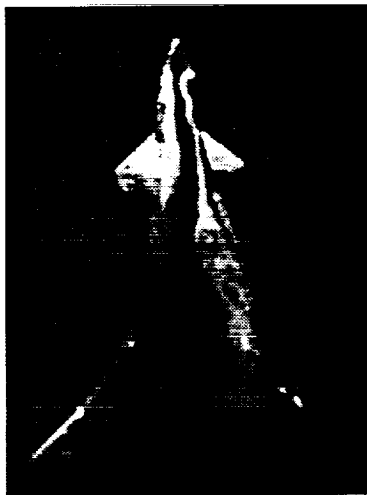
During these tests, the F-18 model showed no unusual activity. Vortex breakdown locations on the forebody vortices, LEX vortices, and wing vortices were found to be symmetric. In addition, no vortex interaction activity was observed. Results of the tests on the X-31 model were not as stable. In fact, the X-31 model showed several instabilities during the same maneuver. Examples of these instabilities are shown below. One of the most easily observable instabilities is the asymmetric forebody vortex position shown on the right. In this case, the starboard side forebody vortex has moved over the canopy to the port side. In addition, both vortices pair together just aft of the port side canard. Another type of instability is shown by the figure on the left. In this figure, asymmetric vortex breakdown has occurred on the forebody vortices. The port side forebody vortex experiences breakdown sooner than the starboard side forebody vortex. Events such as these could provide the initial roll instabilities that lead to self-induced oscillations.



THE HESSERT CENTER

COMPARISON OF F-18 AND X-31 VORTEX POSITION DURING PITCH MANEUVERS

ASYMMETRIC VORTEX BREAKDOWN



X-31 AIRCRAFT
MODEL
PITCHING
FROM
 $\alpha = 10^\circ - 60^\circ$

ASYMMETRIC VORTEX POSITION



COMPARISON OF F-18 AND X-31 VORTEX POSITION DURING PITCH MANEUVERS

If the asymmetric vortex breakdown experienced by the X-31 model during pitch maneuvers is observed from a slightly different angle, more information about the seriousness of the asymmetry can be obtained. From this view it can be noted that the positions of vortex breakdown are quite different for the two forebody vortices. In addition, it was also found that the starboard side vortex is actually lifting away from the surface of the model; however, the port side vortex is still close to the model surface. Such a forebody vortex configuration will surely induce a lateral instability on the model.

The erratic motion of the forebody vortices seems to be mostly dependent upon the forebody configuration. With a flattened forebody cross-section and a low profile canopy, there are no large physical barriers to oppose the movement of the forebody vortices around the fuselage. In addition, the added complexity of the pressure fields and separated flowfields of the canards seems to affect the stability of the the forebody vortices. These factors seem to provide enough evidence of instabilities to initiate self-induced oscillations on the X-31 model.



COMPARISON OF F-18 AND X-31 VORTEX POSITION DURING PITCH MANEUVERS

ASYMMETRIC VORTEX BREAKDOWN

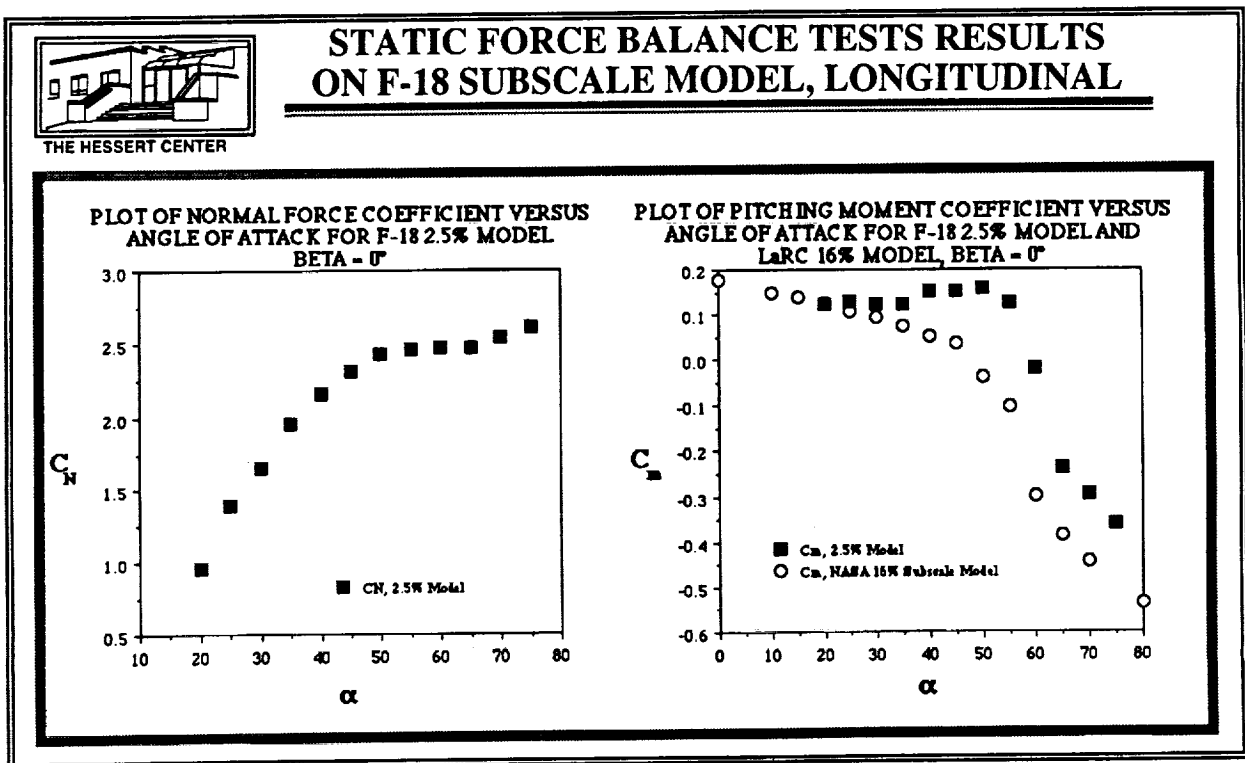


X-31 AIRCRAFT
MODEL
PITCHING
FROM
 $\alpha = 10^\circ - 60^\circ$

STATIC FORCE BALANCE TEST RESULTS ON F-18 SUBSCALE MODEL, LONGITUDINAL

During the pitch testing of the F-18 model, no obvious instabilities were found that could initiate self-induced oscillations. Force balance tests were then conducted to see if the F-18 model was unstable¹⁰.

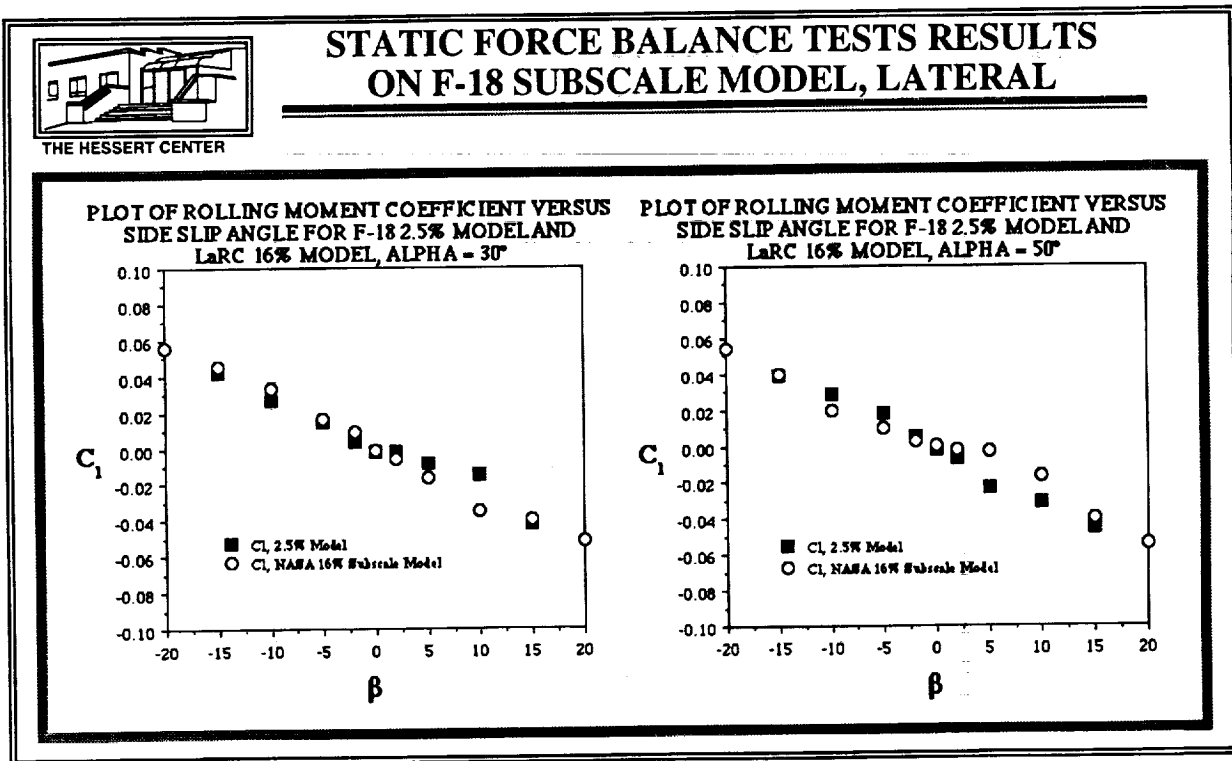
The two longitudinal coefficients, C_N and C_m , are both plotted versus angle of attack. The normal force coefficient, C_N , shows no real surprises. There is a steady increase in the value of the coefficient until $\alpha = 50^\circ$. Then it plateaus between $\alpha = 50^\circ$ and 65° , until the value increases again between $\alpha = 65^\circ$ and 75° . This steady increase in value was expected. The pitching moment coefficient values are compared to 16% subscale F-18 Model tests conducted by NASA⁹. C_m for the 2.5% model was, on average, greater than C_m for the 16% subscale model, reaching its maximum deviation at approximately 50° angle of attack. Thus, in the angle of attack range of 30° to 50° , the aircraft was unstable in pitch. Afterwards, the profile decreases in a similar manner as the full-scale model test, again regaining stability, but at a higher order of magnitude. The reason for this difference in model behavior was found to originate from a difference in surface pressure distribution between the two models.



STATIC FORCE BALANCE TEST RESULTS ON F-18 SUBSCALE MODEL, LATERAL

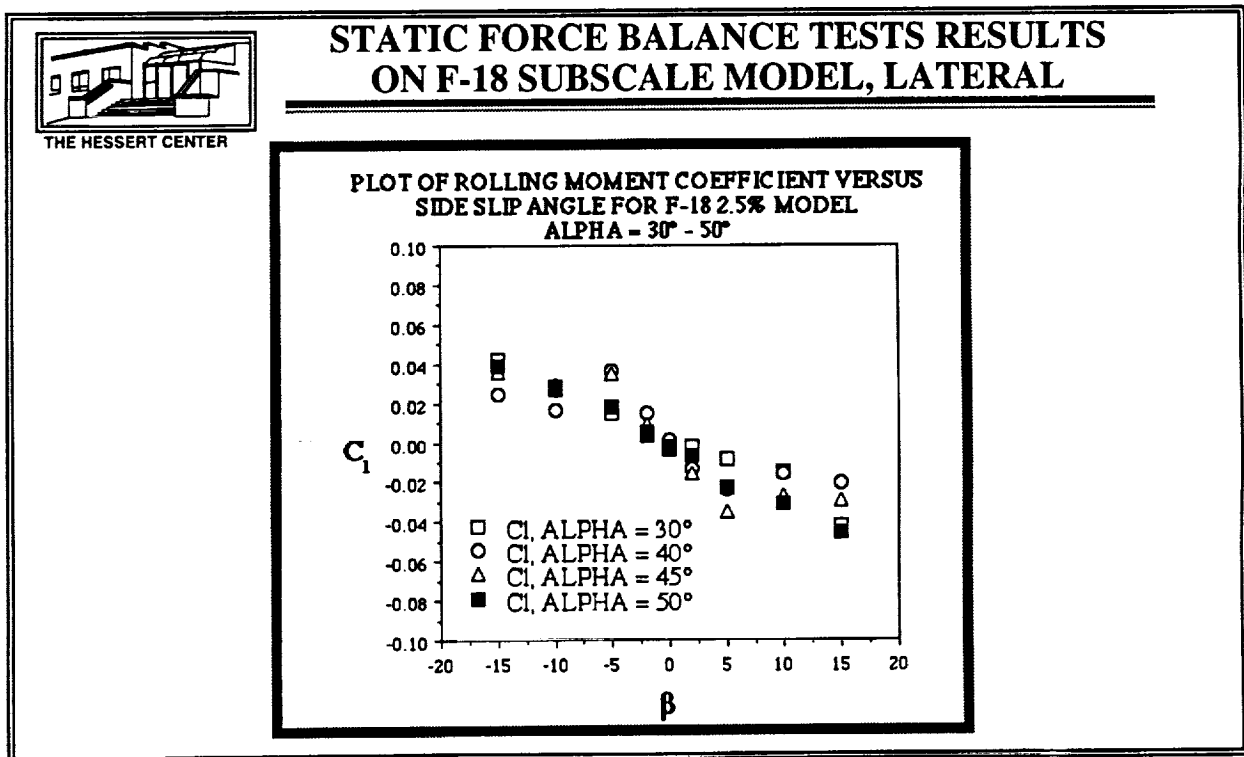
The lateral force and moment coefficients showed very good correlation between the 2.5% F-18 model and the NASA 16% subscale F-18 model⁹. A prime example of this correlation is the rolling moment coefficient, C_l , graphs shown below. For these tests, the values for both the 2.5% and the 16% subscale F-18 models were consistent; and in addition, the slopes of the curves are approximately equal. Thus the rolling moment characteristics of both models are approximately the same as shown by these graphs. In addition, both models showed static stability at these points.

The yawing moment coefficient, C_n , and the side-force coefficient, C_y , were also compared to the results of the 16% subscale F-18 model tests conducted by NASA⁹. In these comparisons, it was also observed that the two models approximated each other very closely in their static lateral behavior¹².



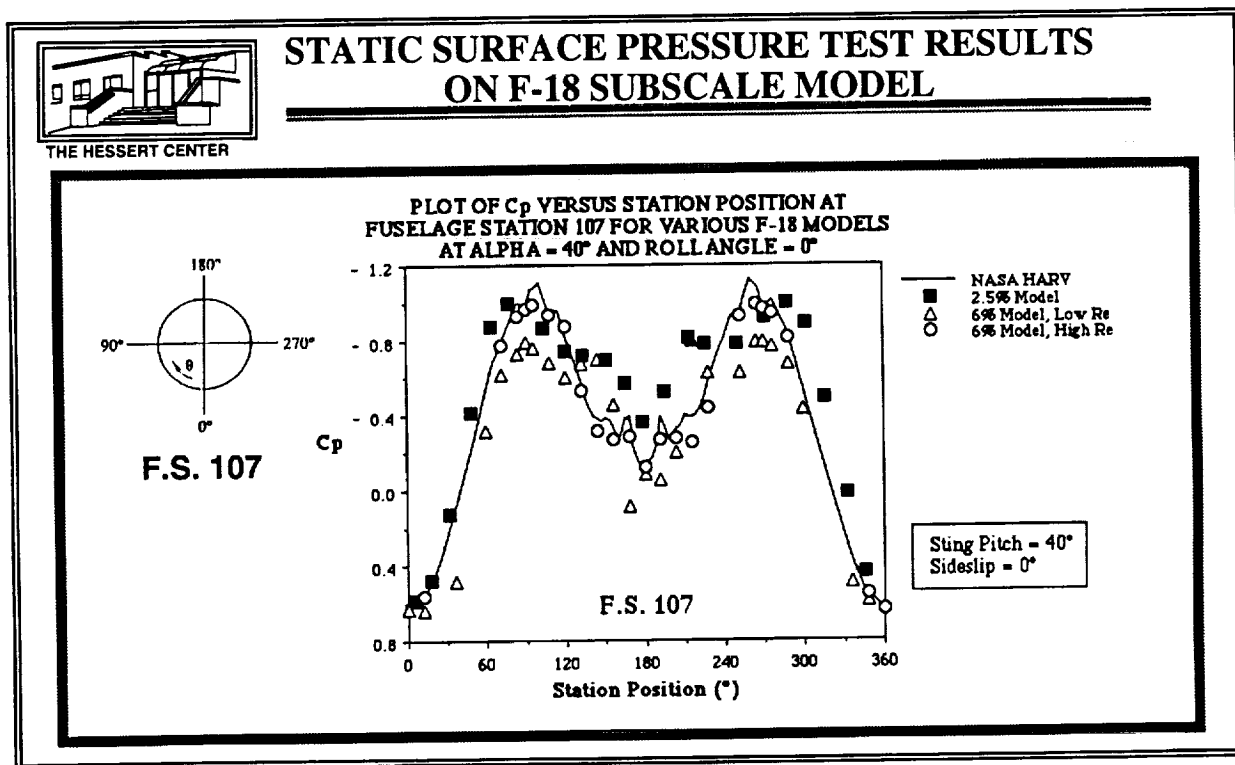
STATIC FORCE BALANCE TEST RESULTS ON F-18 SUBSCALE MODEL, LATERAL

The rolling moment coefficient, C_l , is plotted versus sideslip for various angles of attack, shown below. The four angles of attack chosen were selected from the wing rock boundary shown previously. The roll moment coefficient curves suggest that the model is statically stable (i.e., $C_{l\beta}$ is negative) in roll over the angle of attack range where wing rock occurs. For a model that is constrained to a pure rolling motion, as was the case in the wing rock experiments, an effective sideslip angle is introduced as the model rolls around its longitudinal axis. Thus, the static roll moment characteristics are not the source of the wing rock motion¹⁰. This leads to the conclusion that for the F-18 model the wing rock motion must be due to an instability caused by the rolling motion such as a forebody-LEX vortex interaction during a rolling motion. This is consistent with the ideas suggested by Quast, Nelson, and Fisher in 1991¹¹.



STATIC SURFACE PRESSURE TEST RESULTS ON F-18 SUBSCALE MODEL

Surface pressure measurements conducted on the 2.5% F-18 model¹² were compared to similar information on a 6% F-18 model² and the HARV vehicle⁵. Differences between the HARV and the 2.5% F-18 model pressure coefficient profiles were due mainly to Reynolds number effects. Due to the laminar nature of the 2.5% model tests, the primary separation point on the subscale model occurs earlier than the turbulent primary separation point on the HARV. The first pressure coefficient peak of the HARV is due to the natural acceleration and deceleration of air as it moves around the forebody, whereas the first peak of the model is due to the early primary separation point. Even though two different aerodynamic mechanisms are at work, the profiles compare favorably due to an approximate 30° shift in the pressure coefficient suction peak locations; in addition, both the peaks of the HARV and the 2.5% model are of similar magnitude. Lastly, the leeward pressure recovery region between 150° and 210° compares relatively well, with this region encompassing reattachment points and secondary vortices.



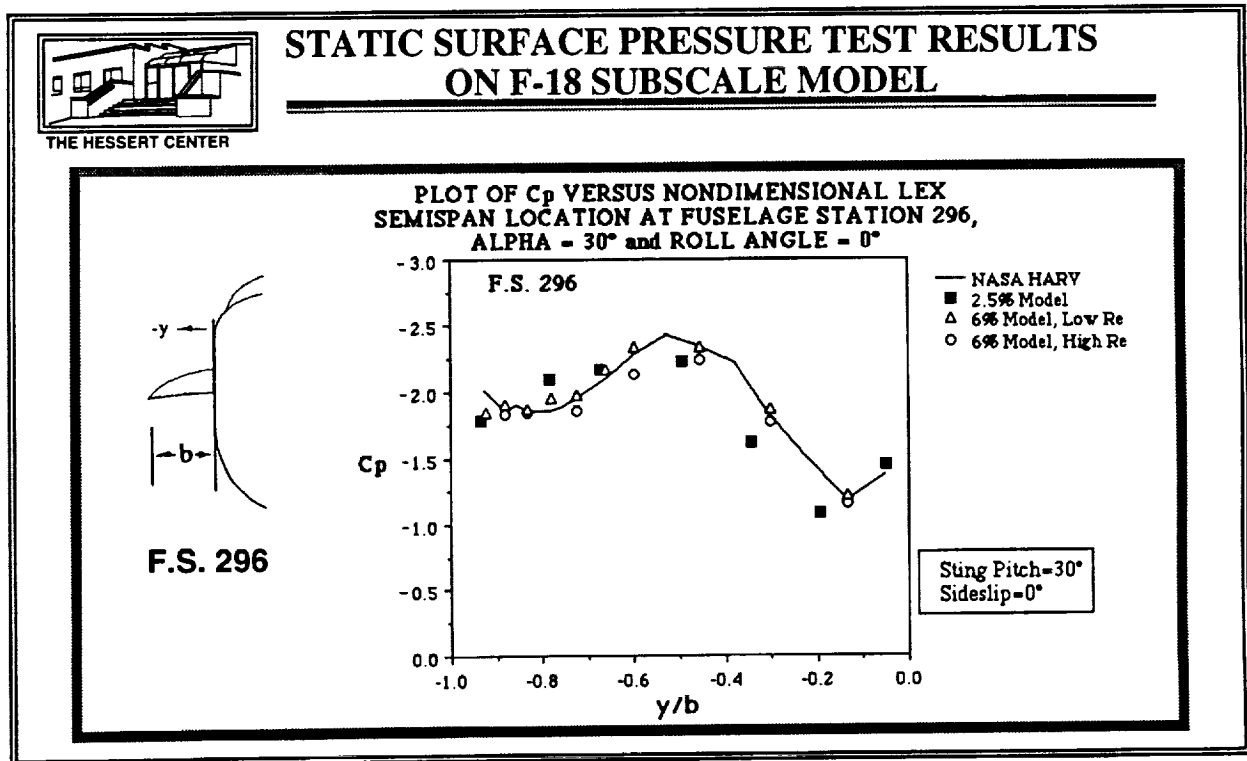
STATIC SURFACE PRESSURE TEST RESULTS ON F-18 SUBSCALE MODEL

Surface pressure distributions over the LEXs of the 2.5% compared very well with those of the HARV vehicle at high alpha^{2,5}. Again most of the difference seen in the profiles can be attributed to Reynolds number or Mach number influences.

The profile for the 2.5% subscale model has two differences when compared to the HARV's pressure coefficient profile. The first is the modification of the leading-edge pressure distribution. This difference is the result of increased strength and size of the secondary vortex due to the laminar boundary layer⁶. The second difference is the location of the maximum suction pressure peak. For the subscale model, this suction pressure peak is further out over the LEX, and is a result of the position of the leading-edge LEX vortex. Thus for the subscale model, the leading-edge LEX vortex is slightly further outboard on the LEX than for the case of the HARV vehicle.

Regardless of these minor differences, the pressure coefficient profiles of both the subscale model and the HARV vehicle are similar; and, the primary separation still dominates the flowfield and the surface pressures.

Since the subscale model demonstrates comparable flowfields to the HARV vehicle, it points out that the stability of the vortices, especially on the forebody, must be of primary importance to the self-induced oscillations.



SIMILARITIES AND DIFFERENCES IN F-18 AND X-31 SUBSCALE MODEL BEHAVIOR

Out of all the subscale model tests conducted, several points of comparison and contrast have emerged between the F-18 and X-31 subscale models. First, the self-induced oscillation envelopes for the models occurs at approximately the same angles-of-attack. The motions experienced within the envelope are different for each model, with the X-31 motions being mainly divergent. Second, the reduced frequencies of the models are of the same order of magnitude. In addition, the F-18 model oscillated at a slightly faster rate than the X-31 model. Third, the models showed different levels of aerodynamic stability during the model pitch tests. The F-18 model showed no asymmetric activity during pitching motions; however, the X-31 model showed several different types of asymmetric instabilities during the same type of pitch tests. Lastly, the forebody vortices on each model had different characteristics during the self-induced motions. The forebody vortices of the F-18 model were found to be stable and to interact with the LEX vortices at large roll angles, $\phi \geq \pm 20^\circ$. The forebody vortices of the X-31 model were found to be easily disturbed and easily moved across the canopy to interact with each other at small roll angles, $\phi = \pm 10^\circ$. Thus each model has similar ranges of self-induced behavior; but, the type and cause of these behaviors is different between the two models.



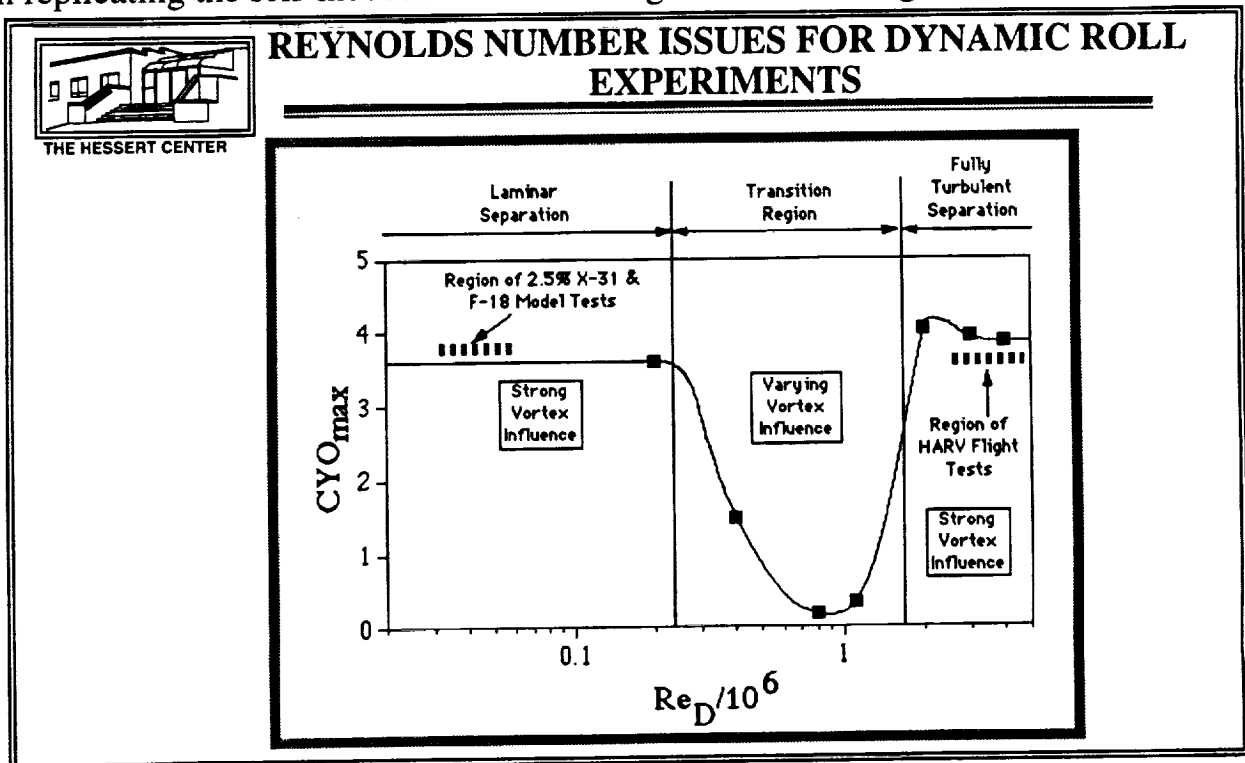
SIMILARITIES AND DIFFERENCES IN F-18 AND X-31 SUBSCALE MODEL BEHAVIOR

Topic	F-18	X-31
Envelope	$\alpha = 30^\circ - 52^\circ$	$\alpha = 30^\circ - 54^\circ$
Reduced Frequency	$f_r = 0.04 - 0.05$	$f_r = 0.02 - 0.03$
Instabilities During Pitch Tests?	NO	YES
Forebody Vortex Motion	Interacts with LEX Vortices at large roll angles.	Easily moves across canopy to interact with each other.

REYNOLDS NUMBER ISSUES FOR DYNAMIC ROLL EXPERIMENTS

In dynamic subscale model testing, a myriad of scaling factors and nondimensional numbers become crucial. During the free-to-roll testing of the F-18 and X-31 subscale aircraft, one factor became increasingly important, Reynolds number. The Reynolds number differences between the HARV vehicle and the 2.5% models were large, two or three orders of magnitude difference. However, this did not keep the subscale tests from replicating the same phenomena found on the flight vehicle.

The reason that subscale tests successfully predicted the flight characteristics is as follows. The roll dynamic characteristic of the two models is driven by the forebody/LEX (F-18) or forebody/canard (X-31) vortex interaction. As shown in the graph below, Reynolds number has an effect on the side-force of a tangent-ogive forebody⁸. As shown, the subcritical and supercritical ranges have very strong and prominent forebody vortex forces and well organized forebody vortices. The transcritical range does not exhibit a well organized vortex flow. Thus, in free-to-roll testing where the model oscillates due to forebody/LEX or forebody/canard vortex interaction, as in the F-18 and X-31 model cases, the transcritical region should be avoided during testing. There will be differences in separation points due to the differences in laminar and turbulent flow around a body; however, the strong and organized forebody vortex flow is maintained. This seems to be the most critical point in replicating the self-induced motions of flight aircraft during subscale model testing.



CONCLUSIONS

Through these subscale tests, several important facts have been reached. First, subscale dynamic testing can be used to predict the roll dynamics of flight vehicles at high angle-of-attack. The agreement of self-induced oscillation envelopes between the subscale wind tunnel tests and flight data is encouraging. Second, from the tests conducted on the subscale models, it appears that the roll dynamic characteristics are governed by forebody/LEX (F-18) or forebody/canard (X-31) vortex interaction. Third, since strong organized vortical flowfields are critical to establish vortex interaction, the transcritical Reynolds number regime should be avoided during model testing. The Reynolds number based on the forebody diameter is of primary importance to create stable, organized vortical forebody flows. Lastly, subscale static aerodynamics agreed favorably with full-scale and other wind tunnel experiments.



THE HESSERT CENTER

CONCLUSIONS

- **Subscale Dynamic Testing can be Used to Predict Roll Dynamics of Flight Vehicles.**
- **Roll Dynamic Characteristics are Governed by Forebody/LEX or Canard Vortex Interactions.**
- **Avoid Transcritical Reynolds Number Regime During Testing. (Based on Forebody Diameter)**
- **Static Aerodynamics Agrees favorably with Full-Scale Wind Tunnel Experiments.**

REFERENCES

- ¹Croom, M.A., et al., "Dynamic Model Testing of the X-31 Configuration for High-Angle-of-Attack Flight Dynamics Research," AIAA 93-3674 CP, August 1993.
- ²Erickson, G.E., et al., "Experimental Investigation of the F/A-18 Vortex Flows at Subsonic Through Transonic Speeds, Invited Paper," AIAA 89-2222, July 1989.
- ³Ericsson, L.E., and Reding, J.P., "Scaling Problems in Dynamic Tests of Aircraft-Like Configurations," AGARD CP-227, Paper 25, February 1977.
- ⁴Fisher, D.F., and Del Frate, J.H., "In-Flight Flow Visualization Characteristics of the NASA F-18 High Alpha Research Vehicle at High Angles of Attack," SAE Technical Paper Series No. 892222, September 1989.
- ⁵Fisher, D.F., Banks, D.W., and Richwine, D.M., "F-18 High Alpha Research Vehicle Surface Pressures: Initial In-Flight Results and Correlation with Flow Visualization and Wind-Tunnel Data," NASA TM-101724, August 1990.
- ⁶Hummel, D., "On the Vortex Formation Over a Slender Wing at Large Angles of Incidence," AGARD CP-247, 1978.
- ⁷Kegelman, J.T., and Roos, F.W., "Influence of Forebody Cross-Section Shape on Vortex Flowfield Structure at High Alpha," AIAA 91-3250, September 1991.
- ⁸Lamont, P.J., "Pressures Around an Inclined Ogive Cylinder with Laminar, Transitional, or Turbulent Separation," *AIAA Journal*, Volume 10, Number 11, Pages 1492 - 1499.
- ⁹Murri, D.G., et al., "Developments of Actuated Forebody Strake Controls for the F-18 High Alpha Research Vehicle," High-Angle-of-Attack Technology Conference, October 1990.
- ¹⁰Nelson, R.C., Arena, A.S., and Williams II, D.L., "The Use of Subscale Models to Predict Self-Induced Oscillations of Flight Vehicles," AIAA 93-0093, January 1993.
- ¹¹Quast, T., Nelson, R.C., and Fisher, D.F., "A Study of High Alpha Dynamics and Flow Visualization for a 2.5% Model of the F-18 HARV Undergoing Wing Rock," AIAA 91-3267, September 1991.
- ¹²Williams II, D.L., Quast, T., and Nelson, R.C., "Comparison of Flight and Sub-scale Model Wing Rock Characteristics of an F-18 Aircraft," Final Report for NASA Grant NCA2-513, April 1993.
- ¹³Williams II, D.L., Nelson, R.C., and Fisher, D.F., "An Investigation of X-31 Roll Characteristics at High Angle-of-Attack Through Subscale Model Testing," AIAA 94-0806, January 1994.
- ¹⁴Villeta, J.R., "Lateral-Directional Static and Dynamic Stability Analysis at High Angles of Attack for the X-31 Configuration," Master's Thesis, George Washington University, August 1992.